Light Scattering Analysis of Upper Critical Solution Temperature Behavior in a Poly(vinylidene fluoride)/Poly(methyl methacrylate) Blend

Hideaki Tomura,† Hiromu Saito, and Takashi Inoue*

Department of Organic and Polymeric Materials, Tokyo Institute of Technology, Ookayama, Meguro-ku, Tokyo 152, Japan

Received April 16, 1991; Revised Manuscript Received October 7, 1991

ABSTRACT: We carried out the light scattering studies under both H_V and V_V optical alignments on the competitive progress of the crystallization and the liquid–liquid phase separation in a blend of poly(vinylidene fluoride) and poly(methyl methacrylate) after the temperature drop from a single-phase melt to various low temperatures. The upper critical solution temperature (UCST) type phase boundary below the melting temperature was determined by the temperature dependence of three kinetic variables of the liquid–liquid phase separation: (1) the initial slope of the time variation of the invariant of V_V scattering, (2) the most probable wavenumber of concentration fluctuation having the highest rate of growth, and (3) the apparent diffusion constant. The critical temperatures estimated by the three different methods agreed well with each other and showed a similar composition dependence. The critical temperature was also determined by a kinetic discussion on the crystallization affected by the liquid–liquid phase separation, and it was found to be nearly equal to those estimated by the three methods. The results strongly justify the UCST type phase behavior. Combining the literature data, the phase diagram of the binary system was drawn in terms of the UCST, the melting point depression, and the LCST (lower critical solution temperature) curves.

Introduction

Poly(vinylidene fluoride) (PVDF) is known to be miscible with poly(methyl methacrylate) (PMMA) at low temperature.[1-7] The mixture tends to phase separate at higher temperatures. The lower critical solution temperature (LCST) is reported to be around 350 °C.[8] Below the melting temperature T_m (~178 °C), PVDF crystallizes from the homogeneous melt.[9-13] At lower temperatures far below T_m, the liquid–liquid phase separation is pointed out to occur by microscopic observation of structure development after the temperature drop to the lower temperatures.[14] This upper critical solution temperature (UCST) type phase behavior is supported by an electron spin resonance study.[15] Thus, UCST locates below T_m so that the crystallization takes place above UCST, and below UCST the liquid–liquid phase separation precedes and the crystallization follows.[14] In such a situation, one is not able to determine the equilibrium point UCST by the conventional cloud-point method. One has to rely upon the kinetic analysis of the competitive progress of the two rate processes.

In this paper, to determine the UCST type phase boundary in a PVDF/PMMA blend, we carry out light scattering studies on the competitive progress of the crystallization and the liquid–liquid phase of the crystallization and the liquid–liquid phase separation at the isothermal setting below T_m after the temperature drop of the single-phase mixture prepared above T_m. The phase boundary is obtained by the kinetic analysis of liquid–liquid phase separation. The result is confirmed by a kinetic aspect of the crystallization affected by the liquid–liquid phase separation.

Experimental Section

The polymer specimens used in this study were commercial polymers. PVDF was supplied by Kureha Chemical Industry Co., Ltd.; KF1000, $M_n = 7.0 \times 10^4$. PMMA was supplied by Mitsubishi Rayon Co., Ltd.; Acrypet M001, $M_w = 11.0 \times 10^4$, $M_n = 5.0 \times 10^4$.

PVDF and PMMA were dissolved at 10 wt % of the total polymer in dimethylformamide. The solution was cast onto a cover glass. The solvent was evaporated under a reduced atmosphere of 10^{-2} mmHg at room temperature. The cast film was further dried under vacuum (10^{-4} mmHg) for 3 days and then at 120 °C for 24 h to completely remove residual solvent. The film specimen thus prepared (ca. 30 μm thick) was melted at 200 °C for 10 min in a hot stage. Then the melt specimen was rapidly quenched to a desired annealing temperature T_a by inserting it into another hot chamber set horizontally on the light scattering stage. A polarized He–Ne gas laser of 632.8-nm wavelength was applied vertically to the film specimen. The scattered light was passed through an analyzer. We employed two optical geometries; one was the H_V geometry in which the optical axis of the analyzer was set perpendicularly to that of the polarizer, and the other was the V_V geometry with a parallel set of the two axes. The angular distribution of scattered light intensity was detected by a one-dimensional photometer with a 46-photodiode array (HASC Co., Ltd.). The scattering profiles in a time slice of 30 ms were measured at appropriate intervals and stored in Forth Engyne computer for further analysis.

Results and Discussion

Typical examples of the scattering profiles are shown in Figure 1. Both H_V and V_V scattering intensities increase with annealing time. The H_V scattering is attributed to the optical anisotropy, while the V_V is attributed to both the optical anisotropy and the density fluctuation. To discuss the kinetic aspects of the crystallization and the liquid–liquid phase separation, it is convenient to employ the integrated scattering intensity, i.e., the invariant Q defined by

$$Q = \int_0^\infty I(q)\, q^2\, dq \qquad (1)$$

where q is the scattering vector, $q = (4\pi/\lambda) \sin(\theta/2)$, λ and θ being the wavelength and scattering angle, respectively, and $I(q)$ is the intensity of the scattered light at q.[16]

The H_V scattering pattern from the crystallized specimen was a four-leaf clover type. It suggests the scattering

* To whom correspondence should be addressed.
† On leave from the Institute of New Materials, Kanebo Co., Ltd., Japan.

0024-9297/92/2225-1611$03.00/0

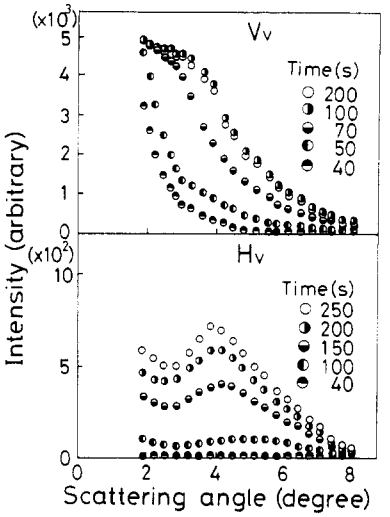

Figure 1. Change of V_V and H_V light scattering profiles with time after the temperature drop for a 60/40 PVDF/PMMA blend at 115 °C.

from spherulites. In this case, the invariant in the H_V mode, Q_{H_V}, is described by the mean-square optical anisotropy $\langle\delta^2\rangle$

$$\langle\delta^2\rangle \propto \phi_s(\alpha_r - \alpha_t)^2 \tag{2}$$

where ϕ_s is the volume fraction of spherulites and α_r and α_t are the radial and tangential polarizabilities of spherulites.[16] On the other hand, the invariant in the V_V mode, Q_{V_V}, is ascribed to both $\langle\delta^2\rangle$, and the mean-square density fluctuation $\langle\eta^2\rangle$. $\langle\eta^2\rangle$ in a neat polymer system is given by

$$\langle\eta^2\rangle = \phi_s(1-\phi_s)(\alpha_c - \alpha_a)^2 \tag{3}$$

where α_c is the average polarizability of the spherulites and α_a is the polarizability of an amorphous matrix. In a phase-separated blend of polymers A and B with a sharp phase boundary, the $\langle\eta^2\rangle$ is similarly described by

$$\langle\eta^2\rangle = \phi_A(1-\phi_A)(\alpha_A - \alpha_B)^2 \tag{4}$$

where ϕ_A is the volume fraction of the A-rich phase and α_i is the polarizability of the i-rich phase.

The time variations of the invariants Q_{H_V} and Q_{V_V} are shown in Figure 2. As shown in Figure 2a, both invariants of neat PVDF gradually increase with the time of annealing. Similar time variations are seen in the 60/40 blend at high T_a, as shown in Figure 2b. Such time variations are typical for the crystallization of polymers. In contrast, as shown in Figure 2c, Q_{V_V} at low T_a rapidly increases to attain a maximum and then levels off, while Q_{H_V} starts to increase after the end point of a rapid increase in Q_{V_V}. Note here a big difference in magnitude between Q_{H_V} and Q_{V_V}, compared with those in parts a and b of Figure 2. The big difference can be ascribed to a large contribution of the density fluctuation by the liquid–liquid phase separation to the overall Q_{V_V}, in addition to the density fluctuation associated with the crystallization as in the case of neat PVDF (and also of the blend at high T_a; Figure 2b). The rapid increase of Q_{V_V} and the slow increase of Q_{H_V} after the time lag in Figure 2c may suggest that the liquid–liquid phase separation precedes and the crystallization follows. In other words, the T_a locates below UCST and the crystallization starts only after the phase separation proceeds to a certain level. Consequently, one can discuss the location of UCST from the relative increase of Q_{V_V} normalized by that of Q_{H_V} as follows.

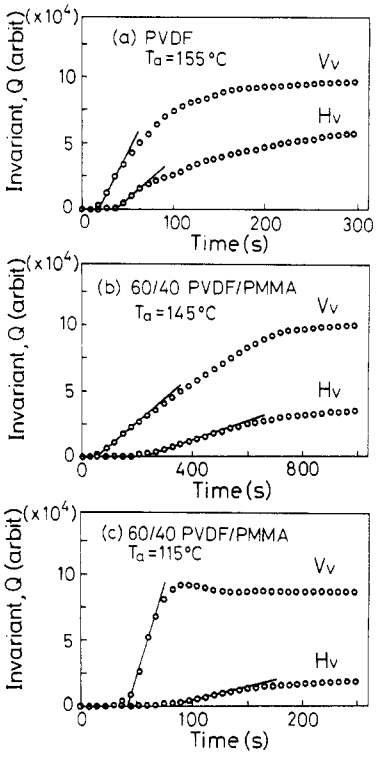

Figure 2. Time variation of invariants Q_{V_V} and Q_{H_V}: (a) neat PVDF at 155 °C, (b) a 60/40 PVDF/PMMA blend at 145 °C, and (c) a 60/40 PVDF/PMMA blend at 115 °C.

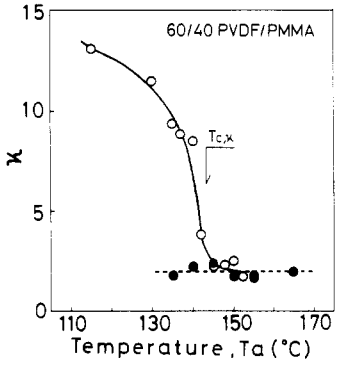

Figure 3. Temperature dependence of κ: neat PVDF (●) and a 60/40 PVDF/PMMA blend (○).

The initial slope of the time variation of Q_{H_V} (see the thin straight line in Figure 2), dQ_{H_V}/dt, is assumed to be a rate constant of crystallization, while dQ_{V_V}/dt is composed of the crystallization rate and the liquid–liquid phase separation rate. A ratio of the two rate constants, $\kappa \equiv (dQ_{V_V}/dt)/(dQ_{H_V}/dt)$, should be a parameter which describes the relative rate of the phase separation.

The value of κ in neat PVDF was estimated to be almost constant at various T_a, as indicated by closed circles in Figure 3. In contrast, the κ value of the blend is estimated to depend very much on T_a. As T_a increases, κ abruptly decreases at $T_{c,\kappa}$ (~142 °C) and then maintains almost the same level as that of neat PVDF at $T_a > T_{c,\kappa}$. It implies that the normal crystallization takes place above $T_{c,\kappa}$, and the liquid–liquid phase separation starts to occur when T_a is decreased below $T_{c,\kappa}$, suggesting the UCST type phase behavior. Values of κ were similarly obtained for the blends with different compositions, and these are plotted by open triangles in Figure 8.

As shown in Figures 1 and 2c, at $T_a < T_{c,\kappa}$, the contribution of the crystallization to the overall V_V scattered light intensity I_{V_V} is assumed to be negligible at

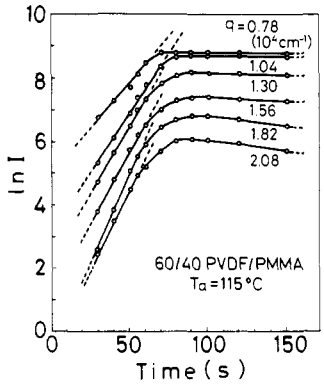

Figure 4. Time variations of the scattered light intensity at various q's for a 60/40 PVDF/PMMA blend at 115 °C.

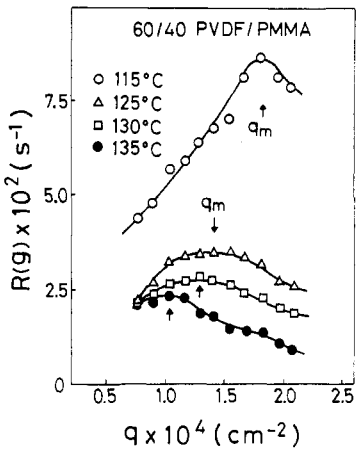

Figure 5. $R(q)$ spectra for 60/40 PVDF/PMMA blends quenched to various temperatures.

early stages. Hence, one can discuss the details of the liquid–liquid phase separation by the initial time variation of I_{V_V} at a time window before the onset of crystallization. According to the linear theory by Cahn,[17] time evolution of the scattered light intensity associated with the spinodal decomposition is described by

$$I_{V_V}(q,t) \propto \exp[2R(q)\cdot t] \tag{5}$$

where t is the time after the initiation of spinodal decomposition and $R(q)$ is the growth rate of concentration fluctuation having wavenumber q, defined by

$$R(q) = -Mq^2(\partial^2 f/\partial\phi^2 + 2Kq^2) \tag{6}$$

where M is the mobility, f is the free energy density of a mixture, and K is the gradient energy coefficient. As expected by eq 5, the exponential increase of I_{V_V} is realized for the blend at $T_a < T_{c,\kappa}$, as shown in Figure 4. Note that the exponential character is one of the hallmarks of spinodal decomposition.

According to eq 5, one can obtain $R(q)$ from the slope of a plot of ln I vs t in Figure 4. The $R(q)$ spectrum obtained had a maximum at q_m, as shown in Figure 5. This is another hallmark of spinodal decomposition. Employing the relationship $-(\partial^2 f/\partial\phi^2) \propto |T_a - T_s|$, the q_m is an increasing function of the quench depth $|T_a - T_s|$[18]

$$q_m^2 \propto |T_a - T_s| \tag{7}$$

where T_s is the spinodal temperature. A plot of q_m^2 as a function of temperature T_a is shown in Figure 7. A linear relationship is obtained as expected from eq 7, and the spinodal temperature T_s ($=T_{s,q}$) was estimated by an intercept of the temperature axis. The values of $T_{s,q}$ for

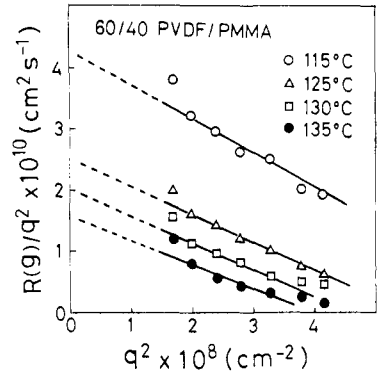

Figure 6. Plots of $R(q)/q^2$ versus q^2 for 60/40 PVDF/PMMA blends quenched to various temperatures.

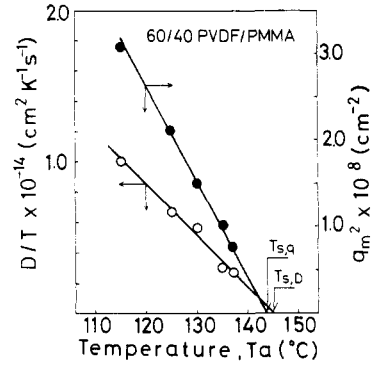

Figure 7. Temperature dependence of q_m^2 and D/T in a 60/40 PVDF/PMMA blend.

various compositions were obtained, and these were plotted by open circles in Figure 8.

T_s can also be obtained from the temperature dependence of the apparent diffusion constant $D = -M(\partial^2 f/\partial\phi^2)$[19]

$$D \propto |T_a - T_s|\cdot T_a \tag{8}$$

which is given by the Stokes–Einstein equation $M \propto T$ and $(\partial^2 f/\partial\phi^2) \propto |T_a - T_s|$.[18] The value of D was estimated by eq 6, i.e., from the intercept of the straight line of the $R(q)/q^2$ versus q^2 plot in Figure 6. A plot of D/T_a versus T_a is shown in Figure 7. A linear relationship is obtained as expected from eq 8. Then, T_s ($=T_{s,D}$) was estimated by an intercept of the temperature axis. The values of $T_{s,D}$ for various compositions were similarly obtained, and these were plotted by closed circles in Figure 8.

Figure 8 is the phase diagram of a PVDF/PMMA system. Note here the three UCST type phase boundaries in terms of $T_{c,\kappa}$, $T_{s,q}$, and $T_{s,D}$ show similar composition dependences. Also shown in Figure 8 are the LCST type phase boundary and the melting point depression curve, reproduced from our previous work[14] and literature,[10] respectively. Furthermore, another UCST type phase boundary is shown by the broken line. The boundary, reproduced also from our previous work,[14] locates slightly lower than that of the present work. It is not surprising, because the former is based upon the microscopic observation whether the morphology development characteristic to the liquid–liquid phase separation becomes obvious or not when T_a is lowered, and hence the judgement may render the slightly lower boundary.

As discussed in Figures 2c and 3, at low temperatures below $T_{c,\kappa}$ or T_s, the liquid–liquid phase separation precedes and the crystallization follows. Such crystallization would differ from the normal one such as in neat PVDF so that one could find out an affect of UCST behavior on the crystallization kinetics. The crystallization

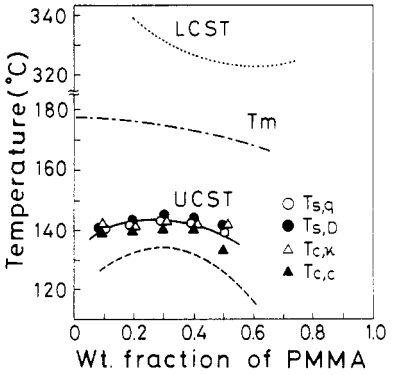

Figure 8. Phase diagram of a PVDF/PMMA system. A UCST type phase boundary is drawn in terms of three kinetic variables of liquid–liquid phase separation; $T_{c,\kappa}$ by a κ vs T_a plot (△), $T_{s,q}$ by q_m vs T_a (○), and $T_{s,D}$ by a D/T vs T_a plot (●). $T_{c,c}$ (▲): critical temperature determined by crystallization kinetics. (The melting point depression curve by a chain line and another UCST phase boundary and LCST phase boundary are reproduced from our previous paper.[14])

after the initiation of the liquid–liquid phase separation will take place in the PVDF-rich region. Such crystallization is expected to be faster than that in a homogeneous mixture, because the degree of supercooling, $\Delta T = T_m - T_a$, should be higher in the PVDF-rich region and the crystallizable (PVDF) chains would be transported to the crystal growth front from the PMMA-rich region under the thermodynamic driving force for the phase separation.

According to the Hoffman–Lauritzen theory on the polymer crystallization,[20,21] the linear growth rate of crystallite G is given by

$$G \propto \beta_g \exp\frac{-K_g}{T_a(\Delta T)f} \tag{9}$$

where β_g is a mobility term which describes the transportation rate of crystallizable molecules to the growth front, K_g is a nucleation constant, and f is the correction factor given by $2T_a/(T_m^0 + T_a)$. At the early stage of crystallization, Q_{H_V} is assumed to be proportional to the volume fraction of crystallite so that the linear growth rate G may be given by

$$G \propto d(Q_{H_V}{}^{1/3})/dt \tag{10}$$

Hence one can estimate G from the initial slope of the time variation of $Q_{H_V}{}^{1/3}$. The values of G estimated by eq 10 are shown as a function of $[T(\Delta T)f]^{-1}$ in Figure 9. In neat PVDF, the temperature dependence is described by two continuous broken lines, while in the blend it is discontinuous and there is a gap at $T_{c,c}$. The gap temperatures are plotted by closed triangles in Figure 8, demonstrating that they locate just below the UCST phase boundary. That is, the growth rate G shows an abrupt increase around T_s as T_a is increased. This is exactly the kinetic aspect discussed above for the crystallization accelerated by the liquid–liquid phase separation.

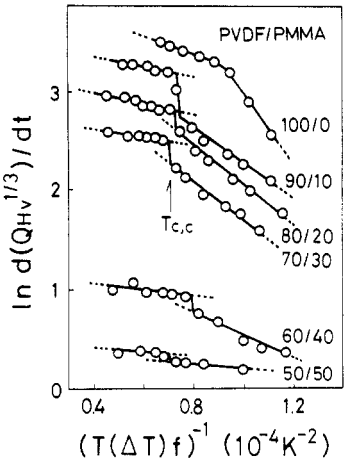

Figure 9. Temperature dependence of the linear crystallization rate estimated by $Q_{H_V}(t)$.

Conclusion

Thus the UCST type phase boundary below the melting temperature was quantitatively determined by the light scattering studies. The critical temperatures obtained by three kinetic analyses of the liquid–liquid phase separation were nearly equal to that obtained by the temperature dependence of the kinetic variable of the crystallization affected by the liquid–liquid phase separation. It supports the validity of these analyses and justifies the UCST phase behavior.

References and Notes

(1) Paul, D. R.; Altamirano, J. O. *Adv. Chem. Ser.* **1975**, *142*, 371.
(2) Hirata, Y.; Kotaka, T. *Polym. J.* **1981**, *13*, 273.
(3) Wendorff, J. H. *J. Polym. Sci., Polym. Lett. Ed.* **1980**, *18*, 439.
(4) Douglass, D. C.; McBrierty, V. J. *Macromolecules* **1978**, *11*, 766.
(5) Ward, T. C.; Lin, T. S. *Adv. Chem. Ser.* **1984**, *206*, 59.
(6) Coleman, M. M.; Zarian, J.; Varnell, D. F.; Painter, P. C. *J. Polym. Sci., Polym. Lett. Ed.* **1977**, *15*, 745.
(7) Roerdink, E.; Challa, G. *Polymer* **1980**, *21*, 509.
(8) Bernstein, R. E.; Cruz, C. A.; Paul, D. R.; Barlow, J. W. *Macromolecules* **1977**, *10*, 681.
(9) Wang, T. T.; Nishi, T. *Macromolecules* **1977**, *10*, 421.
(10) Morra, B. S.; Stein, R. S. *J. Polym. Sci., Polym. Phys. Ed.* **1982**, *20*, 2243.
(11) Morra, B. S.; Stein, R. S. *J. Polym. Sci., Polym. Phys. Ed.* **1982**, *20*, 2261.
(12) Morra, B. S.; Stein, R. S. *Polym. Eng. Sci.* **1984**, *24*, 311.
(13) Leonard, C.; Halary, J. L.; Monnerie, L.; Broussoux, D.; Servet, B.; Micheron, F. *Polym. Commun.* **1983**, *24*, 110.
(14) Saito, H.; Fujita, Y.; Inoue, T. *Polym. J.* **1987**, *19*, 405.
(15) Shimada, S.; Hori, Y.; Kashiwabara, H. *Macromolecules* **1988**, *21*, 3454.
(16) Koberstein, J.; Russel, T. P.; Stein, R. S. *J. Polym. Sci., Polym. Phys. Ed.* **1979**, *17*, 1719.
(17) Cahn, J. W. *J. Chem. Phys.* **1965**, *42*, 93.
(18) Hashimoto, T.; Kumaki, J.; Kawai, H. *Macromolecules* **1983**, *16*, 641.
(19) Inoue, T.; Ougizawa, T. *J. Macromol. Sci., Chem.* **1989**, *A26*, 147.
(20) Lauritzen, J. R., Jr.; Hoffman, J. D. *J. Appl. Phys.* **1973**, *44*, 4340.
(21) Hoffman, J. D.; Frolen, L. J.; Ross, G. S.; Lauritzen, J. I., Jr. *J. Res. Natl. Bur. Stand.* **1975**, *79A*, 671.

Registry No. PVDF, 24937-79-9; PMMA, 9011-14-7.